Nonlamellar Phases in Asymmetric Rod−Coil Block Copolymers at Increased Segregation Strengths

Bradley D. Olsen and Rachel A. Segalman*

Department of Chemical Engineering and Materials Science Division, Lawrence Berkeley Laboratory, University of California, Berkeley, California 94720

Received April 27, 2007; Revised Manuscript Received June 12, 2007

ABSTRACT: A new phase consisting of rectangular rod nanodomains packed onto a hexagonal lattice is observed in rod−coil block copolymers at the limit of both large volume fraction asymmetry and large geometrical asymmetry between the rod and coil. In moderately segregated poly(alkoxyphenylenevinylene-*b*-isoprene) (PPV-*b*-PI), an order−order transition is observed between hexagonal and lamellar phases for polymers near the phase boundary, and the lamellar phase is observed at high temperatures. The domain spacings of polymers in the lamellar phase collapse on to a simple scaling relationship where domain spacing is proportional to molecular weight. The proportionality constant is equal to the statistical segment length of the PPV rod block, suggesting that the angle between the rod director and the lamellar interface is nearly 90°. At higher temperatures, the block copolymers transition from ordered to nematic to isotropic states, with the intermediate nematic phase being observed for all coil fractions studied. A three-dimensional phase diagram shows the microphase and liquid crystalline transitions in rod−coil block copolymers as a function of temperature, geometrical asymmetry, and coil fraction.

Introduction

Rod−coil block copolymers are a promising route to self-assembled nanostructured phases[1−3] for applications in organic electronics and biomaterials. Materials for LEDs and photovoltaics have been prepared using semiconducting conjugated rod−coil block copolymers, where the conjugated structure of the semiconducting polymer provides the rigid block.[4−10] Helical domains in biopolymers also have a rodlike structure, and rod−coil biopolymers have been investigated for several applications.[11−14] The translation of self-assembly principles developed for the more traditional coil−coil block copolymers to these novel rod−coil block copolymer systems is nontrivial due to differences in chain topology and the presence of additional liquid crystalline interactions between the rod blocks. These features fundamentally alter the physics of rod−coil systems and have resulted in the observation of a number of phases not seen in coil−coil block copolymers. Solution and thermally self-assembled materials have demonstrated wavy lamellar,[15] zigzag,[15] arrowhead,[15] lamellar,[16,17] perforated lamellar,[17−19] hexagonal strip,[16,20,21] and puck phases.[17,20−22] Transitions from the microphase separated state to liquid crystalline or isotropic states have been observed in oligomeric materials,[16,17,23] and a weakly segregated polymeric system has been shown to possess thermally reversible transitions between lamellar, nematic, and isotropic phases.[24,25]

Theoretical studies suggest that the lack of more complex phases in the weak segregation limit for rod−coil block copolymers arises form the higher dimensionality of phase space in a rod−coil system. Coil−coil block copolymers can be characterized primarily by the coil fraction, ϕ, and the Flory−Huggins interaction between the blocks, χN.[3] In rod−coil block copolymer systems the liquid crystalline interactions and the topological disparity between the rod and the coil polymer require the introduction of two additional parameters. The Maier−Saupe interaction, μN, characterizes the aligning interactions between the rod blocks. A second geometrical asymmetry parameter, ν, is used to characterize the difference in scaling behavior between the rod and coil.[26−30] The rod and coil blocks of the copolymer are constrained to occupy the same interfacial area. However, their different scaling dimensions imply that their aspect ratios scale differently with molecular weight, creating a packing frustration due to size mismatch. This geometrical parameter, ν, is defined as a ratio between the coil radius of gyration and the rod length. In this manner both ν and ϕ have an impact on the relative interfacial area of the rod and coil and thus the curvature of the equilibrium microphase. Differences in ν may provide an explanation for some of the discrepancies between the oligomeric studies and the higher molecular weight polymers. Prior studies of oligomeric rod−coil materials demonstrate that tuning the molecular weight or coil Kuhn length, both causing changes in ν, results in changes in the microphase structure.[22,31] In addition, increasing molecular weight in mesogen-jacketed polymeric rod−coil materials has been shown to induce a transition between lamellar and hexagonally perforated lamellar phases.[19] However, these structural changes were not been quantified in terms of changing ν in either study.

Prior work on the PPV-*b*-PI model rod−coil system has demonstrated accessible order−disorder transitions (ODTs) and liquid crystalline clearing transitions in these materials and a phase diagram in the weakly segregated limit.[24,25] Only lamellar phases are observed within the microphase-separated region, and nematic and isotropic phases are observed above the ODT. However, ν was dependent on coil fraction in this study, so the resulting phase diagram represents only a two-dimensional slice through the full phase space. The current work extends the study of the PPV-*b*-PI system into the moderate segregation regime by increasing the number of repeat units per chain, N. This increase in chain length causes a significant change in ν at a given coil fraction, resulting in block copolymers with a higher geometrical asymmetry between rod and coil. Hexagonal phases occur in polymers with sufficiently high asymmetry in both ϕ and ν, illustrating the critical importance of both terms in determining the microphase structure of rod−coil block co-

* Corresponding author: e-mail segalman@berkeley.edu.

10.1021/ma070976x CCC: $37.00
Published on Web 08/15/2007

Table 1. Molecular Parameters for PPV-*b*-PI Block Copolymers

block copolymer	PPV M_n (g/mol)	PI M_n (g/mol)	N	ϕ	ν	rod length (nm)	coil R_g (nm)	block copolymer contour length (nm)
PPVbPI-31	5600	2300	109	0.31	0.153	10.51	1.55	25.7
PPVbPI-41	5300	3400	120	0.41	0.196	9.87	1.86	31.8
PPVbPI-56	5600	6600	172	0.56	0.257	10.54	2.61	53.5
PPVbPI-73	5600	13700	277	0.73	0.371	10.54	3.77	100.4
PPVbPI-81	5300	20000	364	0.81	0.477	9.87	4.56	140.8
PPVbPI-87	5600	34400	581	0.87	0.587	10.54	5.98	236.3
PPVbPI-91	5600	50400	815	0.91	0.713	10.51	7.24	341.3

polymers. The scaling behavior of domain size is also examined as a function of both of these parameters, showing a simple collapse onto a scaling relationship that depends only on molecular weight for both weakly and moderately segregated polymers. Liquid crystalline transitions and ODTs are investigated in the higher molecular weight materials and are summarized in a three-dimensional phase diagram for the rod−coil system.

Experimental Methods

Synthesis. Synthesis of poly(2,5-di(2′-ethylhexyloxy)-1,4-phenylenevinylene) (DEH−PPV) was performed as described previously.[24] This Siegrist polycondensation[4,32] produces low-polydispersity PPV with few chemical defects in the rodlike polymer backbone. Three different batches of PPV homopolymer were used for block copolymer synthesis. All PPVs were crystalline below 80 °C, and their liquid crystalline clearing temperatures ranged from 266 to 280 °C, as determined by differential scanning calorimetry (DSC) and polarized optical microscopy (POM).[33] Poly(1,4-isoprene) (PI) was synthesized anionically in benzene, resulting in ∼93% 1,4 addition. The living PI anion was quenched with a macroterminator PPV to form the block copolymer and purified by precipitation into methanol and column chromatography, as described previously.[24]

Molecular Weight Determination. Molecular weights were measured on a Waters 2690 gel permeation chromatograph (GPC) with a Viscotek refractive index detector calibrated using PI standards (Table 1). The polydispersity of all PI samples was less than 1.05. The number-average molecular weight of the PPV block was measured by NMR end-group analysis (Table 1), and the polydispersities of the PPVs were estimated to be 1.06−1.15 using polystyrene standards. Because of the hydrodynamics of rodlike molecules,[34,35] these polydispersities represent upper limits on the true PPV polydispersities. N is the number of volumetric repeat units in each block copolymer (one PI monomer used as reference volume), and ϕ is the volume fraction of PI. Rod and coil dimensions were calculated on the basis of bond length and density data.[24] The coil radius of gyration to rod length ratio, ν, is closely related to the geometric parameter used in self-consistent-field theories and is calculated as[26,29]

$$\nu = \frac{b\sqrt{N\phi}}{\sqrt{6}aN(1-\phi)} \tag{1}$$

where a is the coil statistical segment length and b is the rod segment length such that the rod and coil repeat units have equal volumes. For experimental simplicity, this formula differs from that used in prior theoretical works by a factor dependent only on the coil fraction.[26,36]

Characterization. Samples for small-angle X-ray scattering (SAXS) were prepared by annealing polymers in a vacuum oven at 120 °C for 24 h to form 1 mm thick disks and then sealing the sample between Kapton windows. Experiments were performed on beamline 1-4 of the Stanford Synchrotron Radiation Laboratory (SSRL). The beamline was configured with an X-ray wavelength of 1.488 Å and focused to a spot size of ∼0.5 mm diameter. Data were converted to absolute intensities as described previously.[24] Samples for transmission electron microscopy (TEM) were prepared by spin-coating films of ∼70−100 nm thickness from 2% toluene solution onto silicon nitride windows. All samples were annealed under vacuum at 120 °C for 12 h. The polyisoprene blocks were stained by exposure to the vapor from a 2% OsO_4 solution for 1−4 h. Bright-field images were taken immediately after staining on a JEOL 200CX microscope at the National Center for Electron Microscopy operating at an accelerating voltage of 200 kV.

The liquid crystalline behavior of the samples was investigated through POM and depolarized light scattering (DPLS). An Olympus BX51 microscope with crossed polarizers and an Instec HCS302 heat stage was used to image samples as previously described.[24] The liquid crystalline clearing temperature (transition to the isotropic phase) was identified as the point at which the sample lost all optical texture under crossed polarizers. Samples for DPLS were prepared by annealing a sample of polymer at 80 °C overnight in a vacuum oven to form an ∼0.1 mm thick disk and then sealing the sample between two quartz windows. Depolarized light scattering was measured using a previously described instrument.[37] The sample was initially heated above the ODT and all liquid crystalline transitions and annealed for 30 min. The sample was then cooled and reheated at a slow rate of 5 °C/30 min to minimize hysteresis. Intensity and transmission data were taken from the first cooling and second heating pass. Reported values of I/I_0 were normalized by the transmission of the sample. The transition to the isotropic phase was identified as the point at which the DPLS signal dropped to the baseline level.

Results and Discussion

Structure at Higher Molecular Weight and Higher Geometric Asymmetry. The increased geometrical asymmetry present in longer rod−coil block copolymers results in a wider variety of phases than in the weak segregation limit. At low and moderate coil fractions, the longer polymers form lamellar structures, as shown in SAXS patterns in Figure 1a and TEM images in Figure 2a−d. The increased number of scattering peaks observed and their sharpness suggest that the stronger segregation achieved at higher molecular weight results in a higher degree of order than in lower molecular weight samples.[24,25] The domain spacing of the lamellae increases monotonically with coil fraction, as expected for polymers with rod blocks of approximately equal length. While PPVbPI-31 and -56 both show clear higher order peaks indicative of lamellar structure, PPVbPI-41 shows only a weak second-order peak, as is expected for nearly symmetric lamellae in which interference from the lamellar form factor reduces the intensity of or completely eliminates the $2q^*$ reflection.

Qualitatively different defect structures occur in the lamellar microphases at high and low coil fractions. OsO_4 staining for TEM produces light PPV-rich lamellae and dark PI-rich lamellae shown in Figure 2. The lamellar polymers with higher coil fractions (PPVbPI-56 and PPVbPI-73) demonstrate exceptionally straight PPV containing lamellae, and all of the defects are accommodated by breaking of the PPV lamellae, similar to the behavior observed in weakly segregated rod−coil block copolymers.[24] This lamellar rigidity is attributed to the high bending moduli of the rod nanodomains. However, at low coil fractions (PPVbPI-31 and PPVbPI-41), PPV-rich lamellae may be continuous through defects, as exemplified by the branches

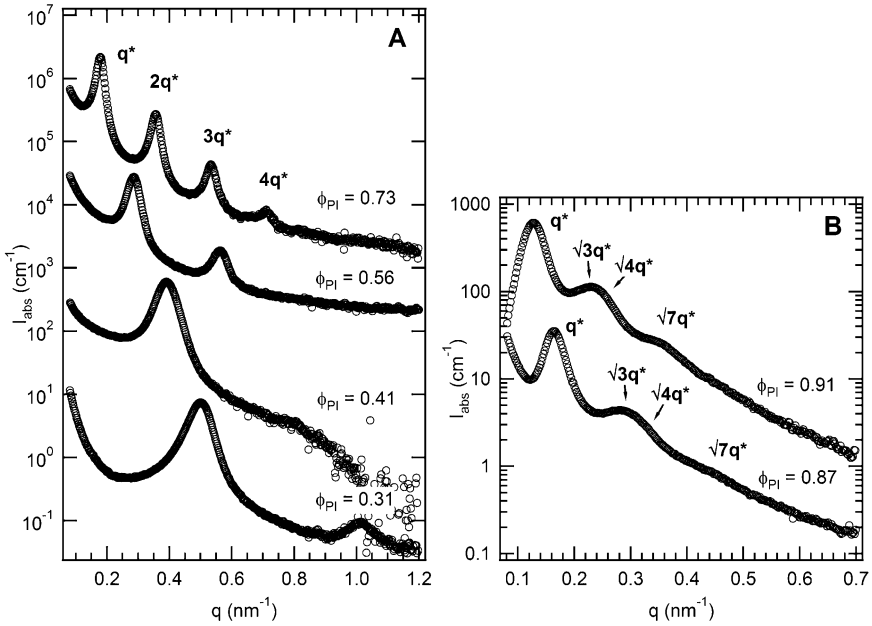

Figure 1. SAXS curves for lamellar and hexagonal morphologies in PPV-*b*-PI. (A) Polymers with coil fractions less than roughly 80% and ν less than 0.4 demonstrate lamellar morphologies with peaks at integer multiples of the primary peak spacing. At 41% PI, only a single peak is clearly observed due to a minimum in the lamellar form factor near the $2q^*$ peak for nearly symmetric lamellae. (B) At higher coil fractions and ν greater than 0.5 the polymers self-assemble into hexagonal phases with peaks at q values of $\sqrt{3}q^*$, $\sqrt{4}q^*$, and $\sqrt{7}q^*$. Curves in both graphs are offset for clarity.

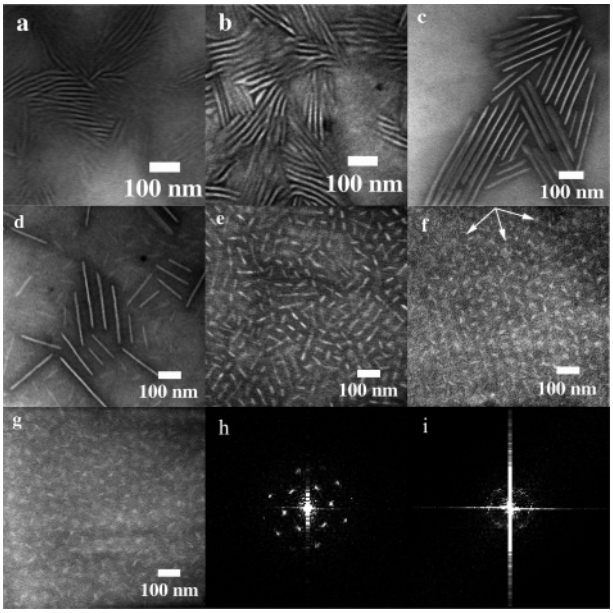

Figure 2. TEM images and Fourier Transforms of PPV-*b*-PI block copolymers. At low coil fractions, the block copolymers self-assemble into lamellae in which dislocations and lamellar dilation are observed in the PPV nanodomains [(a) PPVbPI-31, (b) PPVbPI-41]. At moderate coil fractions the PPV lamellae are exceptionally straight, and all defects are localized to the isoprene nanodomains [(c) PPVbPI-57, (d) PPVbPI-71]. Further increasing coil fraction results in the self-assembly of an intermediate structure where the rod nanodomains form elongated layers with discontinuities similar to hexagonally perforated lamellae [(e) PPVbPI-81]. Finally hexagonally packed structures of small pucklike or striplike aggregates of the rods are observed at the highest coil fractions [(f) PPVbPI-87, (g) PPVbPI-91]. Arrows on the image of PPVbPI-87 indicate the aggregate packing directions in a single crystalline region. OsO_4 staining produces light PPV nanodomains and dark PI nanodomains in all images. Fourier transforms of these polymers show that both have 6-fold symmetries characteristic of a hexagonal structure [(h) PPVbPI-87, (i) PPVbPI-91], but PPVbPI-87 shows a higher degree of order than PPVbPI-91.

in PPV-rich regions that occur at dislocations. In addition, variations in lamellar width are observed along the length of the lamellae. These variations are due to the lower energy compressibe defect modes as compared to bending modes due to the high bending and splay moduli of the liquid crystalline nanodomains, consistent with observations of scanning force microscopy images on the PPV-*b*-PI system.[38] Rod homopolymer shows significantly lower mobility at higher molecular weight,[33] and it seems likely that this lower mobility results in the trapping of both higher energy bending defects and the lower energy dilational defects in the moderately segregated block copolymers with a low coil fraction. Increasing the PI content of the block copolymers increases their mobility, resulting in the disappearance of the higher energy rod bending defects.

At very high coil fractions, PPV-*b*-PI block copolymers self-assemble into hexagonal structures that are not observed in lower molecular weight polymers with similar coil fractions. SAXS patterns, shown in Figure 1b, show overlapping higher order peaks at $\sqrt{3}q^*$ and $\sqrt{4}q^*$ and an additional reflection $\sqrt{7}q^*$ indicative of the hexagonal phase. Similar to the lamellar phase, the domain spacing increases with increasing molecular weight and coil fraction. The structure of these hexagonal phases can be visualized by TEM, as shown in Figure 2f,g. Since the polyisoprene majority phase is stained in these images, contrast between the PPV- and PI-rich phases is weaker than in the lamellar phases. The PPV rods pack into a hexagonal arrangement of nanodomains with rectangular cross sections. The PPV nanodomains show no preferred orientation relative to the lattice directions. This suggests that orientational degrees of freedom are much lower in energy than translational degrees of freedom. An estimate of the rod nanodomain size may be obtained from the TEM image, although the broad interface and staining effects introduce considerable error into this measurement. For PPVbPI-87 where the nanodomain boundaries are clearest, the nanodomains are 31.9 ± 2.5 nm wide and 11.7 ± 0.6 nm thick. Based on an approximate rod diameter of 1 nm, this corresponds to ~1000 rods per nanodomain. This structure is schematically illustrated in Figure 3 with fewer rods per nanodomain for clarity. The PPV domains are more ordered in PPVbPI-87 than PPVbPI-91, as indicated by 2D Fourier transforms of the TEM

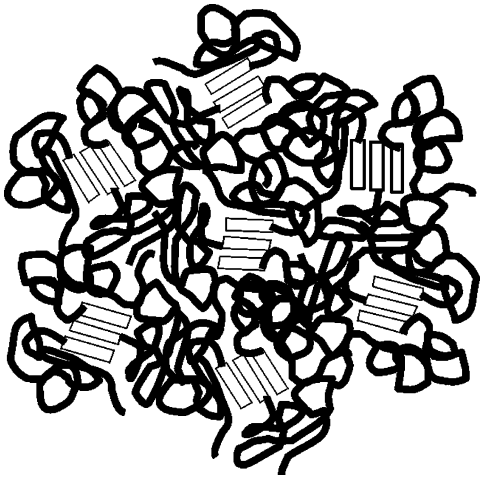

Figure 3. Schematic illustration of the hexagonal phase in PPV-*b*-PI rod−coil block copolymers. At high coil fractions the block copolymers pack onto a hexagonal lattice where the rod nanodomains form rectangular aggregates. Based on the rectangular shape of the aggregates in TEM and the tendency for DEH−PPV to form smectic A phases, the rods directors are drawn perpendicular to the PPV nanodomain interface. While TEM images suggest that there are ∼1000 rods per nanodomain, the schematic is drawn with three rods per nanodomain for clarity.

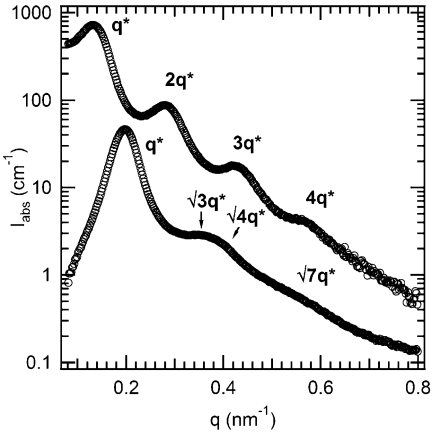

Figure 4. SAXS curves for PPVbPI-81. In between the lamellar and hexagonal regions, the block copolymers show an order−order transition (OOT) between lamellar and hexagonal phases upon heating. When PPVbPI-81 is cast and annealed below the OOT (120 °C), a hexagonal phase (lower curve) is formed. Heating results in an order−order transition to a lamellar phase (upper curve) that is metastable on cooling. Both curves were acquired at 80 °C. Curves are offset for clarity.

images shown in Figure 2h,i. Information from SAXS and TEM would be consistent with either a strip phase, where the aggregates are much longer in the third dimension than the two small dimensions, or a puck phase, where the aggregates are relatively small in all three dimensions. Through TEM we observe no long dimension of the aggregates, which suggests a puck phase.

Around a coil fraction of 0.8, there is a transitional regime between the lamellar and hexagonal phases. In this region, an irreversible order−order transition (OOT) is observed between lamellar and hexagonal phases upon heating. When PPVbPI-81 is cast into a scattering sample and annealed below the ODT to induce ordering, the SAXS pattern shows hexagonal symmetry, as indicated in Figure 4. Heating to160 °C results in an OOT to a lamellar phase, as indicated by a change in the higher order SAXS peak positions to integer multiples of the primary peak position. This phase transition from hexagonal to lamellar is accompanied by a sharp increase in domain spacing. This suggests that the transition between the hexagonal and lamellar phases results from the interplay between the stretching energy of the isoprene block and the desire of the PPV block to form layered phases. The transition from a hexagonal to lamellar phase results in stretching of the PI blocks to accommodate the decreased interfacial area and thus yields an increase in domain size. This higher temperature lamellar phase persists on cooling below 160 °C. Entropic arguments suggest that the decreased area and increased coil stretching present in the lamellar phase should be preferred at low temperature. However, the opposite behavior is experimentally observed, suggesting that chain stretching energy does not motivate this transition, but rather it is driven by the layer-forming tendency of the PPV block.

To determine whether the irreversibility of the OOT results from kinetic trapping or thermodynamic stability of the lamellar phase at low temperature, the polymer was heated in vacuum to above the ODT and then quenched into liquid nitrogen to produce a kinetically trapped disordered structure. This quenched sample was then annealed at 120 °C (below the OOT), and a hexagonal pattern was observed via SAXS. This demonstrates that the hexagonal phase is the thermodynamically stable state at low temperature, and it does not re-form on cooling due to kinetic barriers that trap the polymer in the lamellar state. A sample similarly heated above the OOT under vacuum and recooled slowly to room temperature shows lamellar symmetry by SAXS, confirming that the lamellar phase does not result from sample damage. These observations reinforce the critical importance of distinguishing between thermodynamically reversible and irreversible transitions in rod−coil systems where the kinetic barriers to microphase transitions are very high.

TEM of PPVbPI-81 appears as transitional between the lamellar and hexagonal phases. While the rectangular aggregates apparent in hexagonal polymers are still present, they often align with one another into extended strips, as shown in Figure 2e. These layers appear qualitatively similar to the hexagonally perforated lamellae previously observed in rod−coil[18,19] and coil−coil[39,40] systems, which may be due to the proximity of this polymer to the order−order transition.

The observation of hexagonal phases only at high coil fractions and high geometric asymmetries suggests that control over both parameters is important in rod−coil block copolymers. The dependence of the equilibrium microphase on ν and the coil fraction at room temperature (22−23 °C) is plotted in the phase diagram shown in Figure 5. This phase diagram shows the microphase structure of the seven polymers considered in this study as well as eight polymers from prior work;[24,25] it clearly illustrates that hexagonal phases only occur when there is strong asymmetry in coil fraction and a high relative geometric asymmetry (comparatively low ν). Previously, thermodynamically reversible hexagonal phases had been observed in oligomeric rod−coil materials.[16,20,21,41] The oligomeric rods in these systems have relatively high aspect ratios, and the polymers have a comparatively low value of ν. Discrepancies in this parameter provide a likely explanation for much of the difference in phases observed at a given coil fraction in polymeric and oligomeric materials; decreasing ν in polymeric systems by increasing molecular weight at a constant coil fraction results in closer agreement with the phases seen in oligomeric materials, as illustrated in this study. This is consistent with the SCFT results of Pryamitsyn and Ganesan, where a small decrease in ν promotes the formation of pucklike phases, especially near the ODT.[26] Similar results were also observed using high molecular weight rod−coil polymers based on mesogen-jacketed rod polymers, where increasing the molecular weight lead to preferential formation of hexagonal perforated lamellar phases

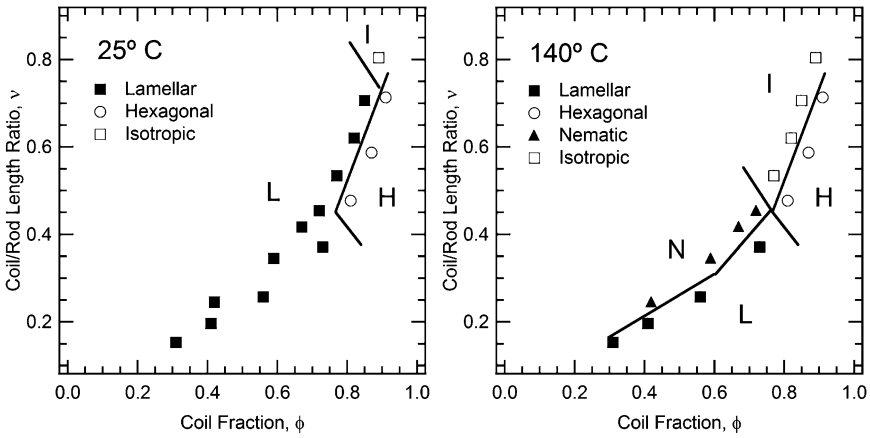

Figure 5. Slices through the PPV-*b*-PI phase diagram in $\phi-\nu$ space. A phase diagram plotted as a function of coil fraction and the coil/rod length ratio shows that lamellar phases are observed across the majority of the experimentally accessible region at 25 °C (room temperature). Increasing both ϕ and ν results in stable hexagonal and isotropic phases. Decreasing ν at constant ϕ is accomplished through an increase in N, resulting in changes in the strength of segregation. Increasing temperature to 140 °C results in the appearance of a nematic window and widening of the isotropic region, while lamellar and hexagonal phases persist at higher ϕ and lower ν.

with more curvature than the standard lamellar phases.[18,19] However, in this system reversible order−disorder transitions could not be used to establish the equilibrium nature of the phases.

Scaling of Domain Size in Rod−Coil Block Copolymers. The scaling of lamellar domain size in rod−coil block copolymers with molecular weight is predicted to differ significantly from that observed in coil−coil block copolymers. In more traditional Gaussian block copolymers, both blocks are flexible. Therefore, as molecular weight of the blocks is increased, coils are free to expand in three dimensions, and scaling goes as $N^{2/3}$ in the strongly segregated limit,[42,43] where N is the number of volumetric repeat units. In contrast, consider a rod−coil block copolymer with rod statistical segment length a, coil fraction ϕ, and a specified rod orientation angle θ relative to the lamellar normal. In the strong segregation limit the width of the rod nanodomain should be equal to the rod length in the direction of the lamellar normal, $Na(1-\phi)\cos\theta$.[30] In the lamellar phase the rod and coil are constrained to occupy equal interfacial area, so the width of the coil nanodomain can be calculated on the basis of the known relative volumes of rod and coil to be $Na\phi\cos\theta$. The total domain spacing is then $Na\cos\theta$. Therefore, scaling theory makes the striking prediction that domain spacing should increase linearly with degree of polymerization across a lamellar phase with constant rod tilt, and the lamellar domain spacing should not depend on the dimensionless parameters ν or ϕ, except through their dependence on N.

Combining results for lamellar domain spacings of both the lower molecular weight weakly segregated materials and the higher molecular weight moderately segregated materials shows that linear scaling of domain spacing with N is observed for polymers with a wide variety of ν and ϕ, as shown in Figure 6. Applying a linear fit restricted to pass through the origin gives a proportionality constant of 0.130 ± 0.004 nm/repeat unit, very close to the calculated rod statistical segment length of 0.135 nm/repeat unit. This indirectly suggests that the rods are oriented nearly perpendicular to the lamellar normal across the coil fractions considered, although small changes in rod tilt or interpenetration of the rod and coil blocks may account for the small difference between the proportionality constant and the statistical segment length. It is important to note that this scaling behavior does not imply that the coils are fully extended or that the coils do not overlap. Rather, the volume occupied by the coil is constant in the plane of the lamellae and grows only in the direction parallel to the lamellar normal. Each coil may be visualized as occupying a cylinder of fixed radius emanating from the rod nanodomains, and as the coil size increases the coil fills a cylinder of increasing length with fixed radius. The coils may still overlap due to overlap between the cylindrical regions that the coils occupy.

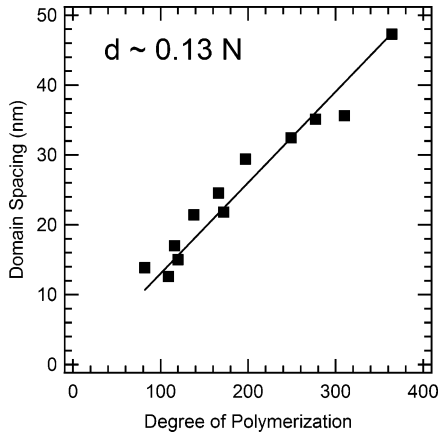

Figure 6. Scaling relationship between domain spacing and molecular weight in lamellar PPV-*b*-PI rod−coil block copolymers. Domain spacing for all the lamellar block copolymers in the weak and moderate segregation regimes shows a linear dependence on N, independent of ϕ and ν. This linear dependence is predicted by scaling theory, and the proportionality constant is very close to the rod statistical segment length, suggesting that the rods are approximately perpendicular to the lamellar interface.

Liquid Crystalline Transitions on Heating. Heating of the polymers from room temperature results in an order to microphase disorder transition (ODT) characterized by both the disappearance of higher order peaks in the SAXS patterns and the divergence of the inverse peak intensity.[25] In these high molecular weight systems the ODT is much sharper than in the low molecular weight systems, as indicated by the sharp divergence of inverse intensity shown in Figure 7. This is expected since density fluctuations are suppressed with increasing molecular weight, leading to a sharper transition in the moderately segregated materials. For lamellar polymers the ODT decreases with decreasing coil fraction until a coil fraction of 0.56 and then increases from 0.56 to 0.73. This likely represents an interplay between the effect of increasing coil fraction on the χN and μN at which the ODT occurs and the effect of an increase in N. Increasing coil fraction is theoretically predicted

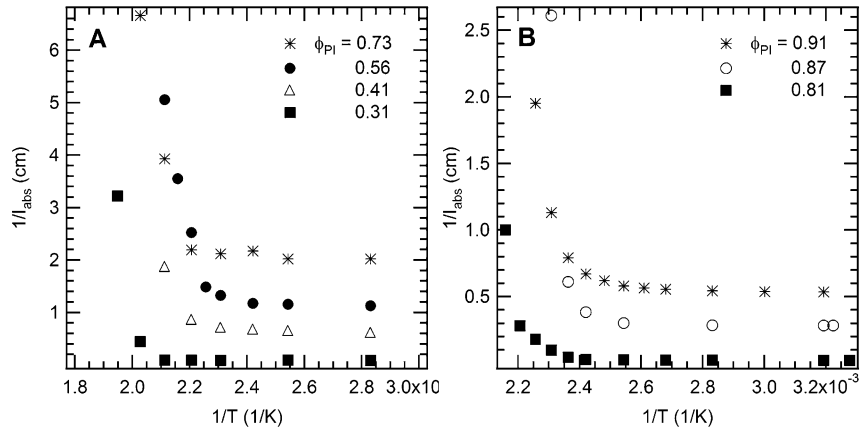

Figure 7. Plots of $1/I$ vs $1/T$ to determine the order to microphase disorder transition (ODT). The ODT is identified as the point at which inverse intensity diverges rapidly in (A) lamellar and (B) hexagonal phases. The ODTs in these higher molecular weight materials are considerably sharper than those for polymers in the weakly segregated limit.

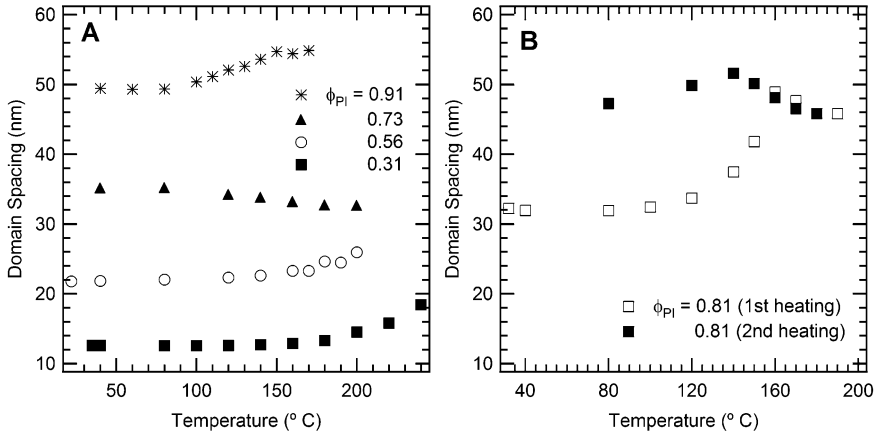

Figure 8. Domain spacing as a function of temperature for PPV-*b*-PI block copolymers. (A) Most PPV-*b*-PI rod−coil block copolymers show an increase in domain spacing on heating. The percentage increase is larger at lower coil fractions in the moderately segregated regime. (B) PPVbPI-81 shows an exceptionally large increase in domain spacing due to the order−order transition between the lamellar and hexagonal phases, and this domain spacing change is irreversible below the OOT due to kinetic trapping of the lamellar phase.

to shift the ODT to higher χN (lower temperature), explaining the steady decrease in ODT between 0.31% and 0.56% coil.[26,28,29] However, increased coil fraction is experimentally achieved by simultaneously increasing the total polymer length, resulting in a higher χN and μN at a given temperature that offsets the incease in coil fraction at high molecular weight and causes the increase in ODT between the coil fractions 0.56 and 0.73.

The domain spacing of PPV-*b*-PI rod−coil polymers changes markedly upon heating. For lamellar materials with a low coil fraction, there is a large percentage increase in domain spacing, as shown in Figure 8a. For PPVbPI-31, this change is a nearly 50% increase. As coil fraction is increased within the lamellar phase, the percentage change in domain spacing decreases, with PPVbPI-73 even showing a small decrease in domain spacing upon heating. Hexagonal materials, with the exception of PPVbPI-81, also show only small increases in domain spacing on heating. These unusual increases in domain spacing with increasing temperature are consistent with observations of more weakly segregated materials that may indicate rearrangements of the rod or coil blocks;[24] however, the coil fractions at which the largest increases in domain spacing are observed are somewhat different.

Unlike all the other block copolymers, the change in domain spacing in PPVbPI-81 is irreversible, as shown in Figure 8b. The large increase in domain spacing corresponds to the OOT where the PI coils must stretch to accommodate the decreased interfacial area per coil, resulting in a rapid increase in domain spacing. This is followed by a slow decrease with further heating up to and above the ODT. Upon cooling the domain size follows a thermally reversible path until the OOT, but below the OOT the polymer diverges onto a second branch with a much larger

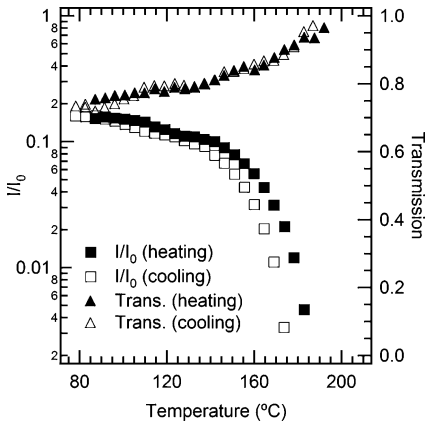

Figure 9. Depolarized light scattering (DPLS) of PPVbPI-91. The persistence of birefringence above the ODT indicates the presence of a narrow nematic region between the ordered and isotropic phases. The ordered phase is characterized by a slow steady drop of DPLS intensity until the ODT (160 °C), at which point the scattered intensity begins to drop much more rapidly. Complete disappearance of DPLS intensity ~20 °C above the ODT indicates the transition from the nematic to the isotropic state.

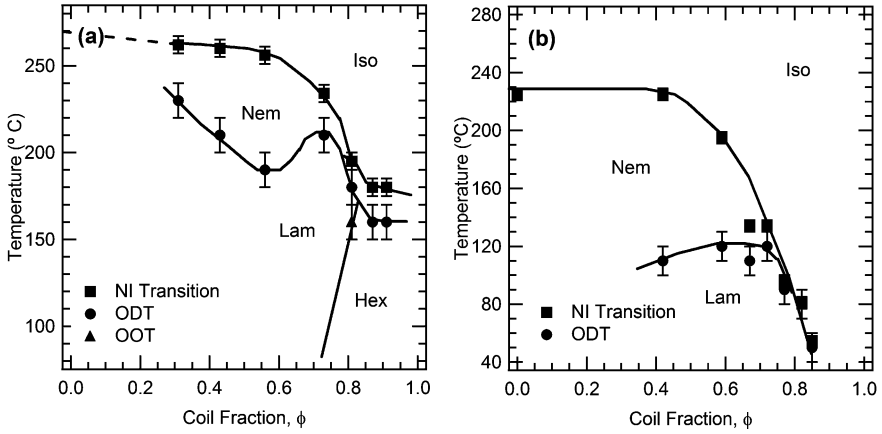

Figure 10. Phase diagram for moderately segregated PPV-*b*-PI. (a) These model rod−coil block copolymers show lamellar phases for low and moderate coil fractions, with hexagonal phases observed at the highest coil fractions. A stable nematic phase is observed above the ODT for all coil fractions, and a transition to the isotropic phase is seen on heating above the nematic. A comparison to the weak segregation limit phase diagram (b) shows that both the ODT increases with increasing segregation strength much more than the nematic−isotropic transition, resulting in a narrow nematic region. However, the nematic phase is stable over a wider range of coil fractions.

domain spacing. This is characteristic of the kinetically trapped lamellar structure.

Heating of the polymers above the ODT results in the formation of aligned nematic phases and eventually isotropic phases. At low/moderate coil fractions, smectic textures are clearly observed under the polarized optical microscope. Heating above the ODT results in a transition to a highly disordered nematic texture, and further heating results in a loss of all birefringence, indicating the transition to the isotropic phase. The liquid crystalline clearing temperature decreases monotonically with increasing coil fraction. At the lowest coil fractions it approaches the clearing temperatures for the rod homopolymer. In contrast to the weakly segregated regime where increasing coil fraction resulted in the disappearance of the nematic phase,[25] a nematic phase is observed above the ODT for all of the moderately segregated hexagonal phases. For these more asymmetric hexagonal polymers (including PPVbPI-81), the birefringence is too weak to accurately detect optical textures under the polarized optical microscope, and so DPLS is used as the primary technique to detect liquid crystalline transitions. A DPLS curve for PPVbPI-91, shown in Figure 9, illustrates that scattered intensity of polarized light decreases slowly below the ODT. Above the ODT the scattered intensity decreases rapidly for ∼20 °C until all birefringence has disappeared, indicating the nematic−isotropic transition. The DPLS curves for these hexagonal PPV-*b*-PIs bear qualitative resemblance to those for high coil fraction weakly segregated PPV-*b*-PIs, but in the weakly segregated case the rapid drop in scattered intensity occurred below the ODT, indicating the absence of a nematic phase.[25] In the higher molecular weight case, the increased rod molecular weight increases the total rod−rod interaction strength (μN) enough to promote the formation of a nematic phase across a wider compositional range. However, the nematic region is much narrower at low coil fractions than in the weakly segregated limit where ν is smaller,[24] a result that is qualitatively consistent with SCFT simulations.[26]

Data on the order−order transition (OOT), ODTs, and liquid crystalline clearing transitions in PPV-*b*-PI are compiled into a phase diagram in the moderate segregation regime, as shown in Figure 10. This phase diagram shows a wide lamellar region at low and moderate coil fractions with a hexagonal region at high coil fractions. The OOT line has a positive slope since the lamellar phase is stable at higher temperatures. A stable nematic region exists above the ODT for all compositions, although this region narrows with increasing coil fraction. Variations in the

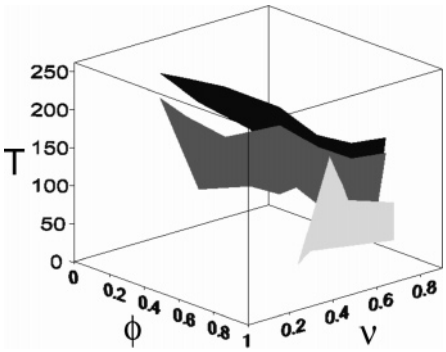

Figure 11. 3D phase diagram for a rod−coil system. The black surface represents the nematic−isotropic transition, the dark gray surface represents the order to microphase disorder transition, and light gray surface represents the lamellar to hexagonal order−order transition. Above the OOT (obscured by the light gray surface) the polymer is in the lamellar phase, and the termination of the OOT surface (light gray) at the ODT surface (dark gray) represents the boundary of the direct hexagonal to nematic transition.

phase structure of these PPV-*b*-PI block copolymers are mapped by a single three-dimensional phase diagram with variable T, ν, and ϕ, shown in Figure 11. Slices through this phase diagram parallel to the $\phi-\nu$ plane are shown in Figure 5 at both room temperature and 140 °C. These phase diagrams clearly illustrate the very large lamellar region with hexagonal phases occupying only a small corner at high geometrical and volume fraction asymmetry. There is a stable nematic region above the ODT except in the weakly segregated limit at high coil fractions where it pinches off, resulting in a direct ordered to isotropic transition.

Conclusions

The effects of increasing geometrical asymmetry and segregation strength on the structure and thermodynamics of rod−coil block copolymers were explored in the moderate segregation limit using a model system PPV-*b*-PI. It was shown that increasing the geometrical asymmetry between the rod and coil as well as the asymmetry between rod and coil volume fraction leads to the formation of hexagonally packed phases of rectangular nanodomains in the coil-rich limit. An order−order transition between lamellar and hexagonal phases was observed for polymers near the boundary between the lamellar and hexagonal regions, with the lamellar phase being preferred at high temperatures. The description of this self-assembly behavior in terms of dimensionless parameters characterizing the mo-

lecular size provides a bridge between studies of oligomeric and polymeric rod−coil systems. The scaling theory of domain spacing was tested, validating the behavior that the domain spacing at constant temperature scales linearly with molecular weight. The proportionality between domain spacing and molecular weight was found to be very close to the theoretically predicted rod statistical segment length. Heating of these polymers results in transitions from ordered to nematic and then isotropic phases. The phase diagram at moderate composition differs from the weak segregation limit in that the nematic region is much more narrow, but a stable nematic phase persists across all observed coil fractions for the higher molecular weight polymers. Finally, a 3D phase diagram has been assembled that shows the phase behavior across a large range of experimentally accessible temperatures and compositions.

Acknowledgment. We gratefully acknowledge support from an NSF-CAREER Award, the ACS-Petroleum Research Fund, and the Department of Energy Office of Basic Energy Sciences through the Plastic Electronics Program at Lawrence Berkeley National Lab (LBNL). SAXS experiments were performed at the Stanford Synchrotron Radiation Laboratory, a national user facility operated by Stanford University, and TEM experiments were performed at the National Center for Electron Microscopy at LBNL, both supported by the Department of Energy, Office of Basic Energy Sciences. We gratefully acknowledge Nitash Balsara for use of the DPLS and John Pople for experimental assistance with SAXS. B. D. Olsen thanks the Fannie and John Hertz Foundation for a graduate fellowship.

References and Notes

(1) Segalman, R. A. *Mater. Sci. Eng., R* **2005**, *48*, 191−226.
(2) Castelletto, V.; Hamley, I. W. *Curr. Opin. Solid State Mater. Sci.* **2004**, *8*, 426−438.
(3) Bates, F. S.; Fredrickson, G. H. *Phys. Today* **1999**, *52*, 32−38.
(4) de Boer, B.; Stalmach, U.; van Hutten, P. F.; Melzer, C.; Krasnikov, V. V.; Hadziioannou, G. *Polymer* **2001**, *42*, 9097−9109.
(5) Van De Wetering, K.; Brochon, C.; Ngov, C.; Hadziioannou, G. *Macromolecules* **2006**, *39*, 4289−4297.
(6) Lin, H. C.; Lee, K. W.; Tsai, C. M.; Wei, K. H. *Macromolecules* **2006**, *39*, 3808−3816.
(7) Hulvat, J. F.; Sofos, M.; Tajima, K.; Stupp, S. I. *J. Am. Chem. Soc.* **2005**, *127*, 366−372.
(8) Yu, W. L.; Meng, H.; Pei, J.; Huang, W.; Li, Y. F.; Heeger, A. J. *Macromolecules* **1998**, *31*, 4838−4844.
(9) Lu, S.; Liu, T. X.; Ke, L.; Ma, D. G.; Chua, S. J.; Huang, W. *Macromolecules* **2005**, *38*, 8494−8502.
(10) Sivula, K.; Ball, Z. T.; Watanabe, N.; Frechet, J. M. J. *Adv. Mater.* **2006**, *18*, 206−210.
(11) Minich, E. A.; Nowak, A. P.; Deming, T. J.; Pochan, D. J. *Polymer* **2004**, *45*, 1951−1957.
(12) Yoda, R.; Komatsuzaki, S.; Nakanishi, E.; Kawaguchi, H.; Hayashi, T. *Biomaterials* **1994**, *15*, 944−949.
(13) Lecommandoux, S.; Achard, M. F.; Langenwalter, J. F.; Klok, H. A. *Macromolecules* **2001**, *34*, 9100−9111.
(14) Ibarboure, E.; Rodriguez-Hernandez, J.; Papon, E. *J. Polym. Sci., Part A: Polym. Chem.* **2006**, *44*, 4668−4679.
(15) Chen, J. T.; Thomas, E. L.; Ober, C. K.; Mao, G. P. *Science* **1996**, *273*, 343−346.
(16) Lee, M.; Cho, B. K.; Kim, H.; Yoon, J. Y.; Zin, W. C. *J. Am. Chem. Soc.* **1998**, *120*, 9168−9179.
(17) Ryu, J. H.; Oh, N. K.; Zin, W. C.; Lee, M. *J. Am. Chem. Soc.* **2004**, *126*, 3551−3558.
(18) Li, C. Y.; Tenneti, K. K.; Zhang, D.; Zhang, H. L.; Wan, X. H.; Chen, E. Q.; Zhou, Q. F.; Carlos, A. O.; Igos, S.; Hsiao, B. S. *Macromolecules* **2004**, *37*, 2854−2860.
(19) Tenneti, K. K.; Chen, X. F.; Li, C. Y.; Tu, Y. F.; Wan, X. H.; Zhou, Q. F.; Sics, I.; Hsiao, B. S. *J. Am. Chem. Soc.* **2005**, *127*, 15481−15490.
(20) Radzilowski, L. H.; Stupp, S. I. *Macromolecules* **1994**, *27*, 7747−7753.
(21) Radzilowski, L. H.; Carragher, B. O.; Stupp, S. I. *Macromolecules* **1997**, *30*, 2110−2119.
(22) Cho, B. K.; Chung, Y. W.; Lee, M. *Macromolecules* **2005**, *38*, 10261−10265.
(23) Radzilowski, L. H.; Wu, J. L.; Stupp, S. I. *Macromolecules* **1993**, *26*, 879−882.
(24) Olsen, B. D.; Segalman, R. A. *Macromolecules* **2005**, *38*, 10127−10137.
(25) Olsen, B. D.; Segalman, R. A. *Macromolecules* **2006**, *39*, 7078−7083.
(26) Pryamitsyn, V.; Ganesan, V. *J. Chem. Phys.* **2004**, *120*, 5824−5838.
(27) Singh, C.; Goulian, M.; Liu, A. J.; Fredrickson, G. H. *Macromolecules* **1994**, *27*, 2974−2986.
(28) Holyst, R.; Schick, M. *J. Chem. Phys.* **1992**, *96*, 730−740.
(29) Matsen, M. W.; Barrett, C. *J. Chem. Phys.* **1998**, *109*, 4108−4118.
(30) Semenov, A. N. *Mol. Cryst. Liq. Cryst.* **1991**, *209*, 191−199.
(31) Cho, B. K.; Lee, M.; Oh, N. K.; Zin, W. C. *J. Am. Chem. Soc.* **2001**, *123*, 9677−9678.
(32) Kretzschmann, H.; Meier, H. *Tetrahedron Lett.* **1991**, *32*, 5059−5062.
(33) Olsen, B. D.; Jang, S. Y.; Luning, J. M.; Segalman, R. A. *Macromolecules* **2006**, *39*, 4469−4479.
(34) Ortega, A.; de la Torre, J. G. *J. Chem. Phys.* **2003**, *119*, 9914−9919.
(35) Riseman, J.; Kirkwood, J. G. *J. Chem. Phys.* **1950**, *18*, 512−516.
(36) The differences in how n is calculated between our work and the theoretical work creates qualitative differences in the behavior of n with changing coil fraction and molecular weight. Increasing molecular weight at constant coil fraction always results in a decrease in ν. However, changes in coil fraction are experimentally accomplished by increasing the coil molecular weight at constant rod molecular weight. This results in an increase in n in our calculation scheme but a decrease in n in the theoretical scheme.
(37) Garetz, B. A.; Newstein, M. C.; Dai, H. J.; Jonnalagadda, S. V.; Balsara, N. P. *Macromolecules* **1993**, *26*, 3151−3155.
(38) Olsen, B. D.; Li, X.; Wang, J.; Segalman, R. A. *Macromolecules*, **2007**, *40*, 3287−3295.
(39) Vigild, M. E.; Almdal, K.; Mortensen, K.; Hamley, I. W.; Fairclough, J. P. A.; Ryan, A. J. *Macromolecules* **1998**, *31*, 5702−5716.
(40) Hajduk, D. A.; Takenouchi, H.; Hillmyer, M. A.; Bates, F. S.; Vigild, M. E.; Almdal, K. *Macromolecules* **1997**, *30*, 3788−3795.
(41) Lee, M.; Kim, J. W.; Hwang, I. W.; Kim, Y. R.; Oh, N. K.; Zin, W. C. *Adv. Mater.* **2001**, *13*, 1363−1368.
(42) Matsen, M. W.; Bates, F. S. *Macromolecules* **1996**, *29*, 1091−1098.
(43) Semenov, A. N. *Zh. Eksp. Teor. Fiz.* **1985**, *88*, 1242−1256.

MA070976X